Available online at www.sciencedirect.com
ScienceDirect
Journal of Sound and Vibration 301 (2007) 400–409
JOURNAL OF SOUND AND VIBRATION
www.elsevier.com/locate/jsvi

Short Communication

Wind-excited overhead transmission lines: Estimation of connection stresses at junctions

Nandan Kumar Sinha[a,*], Peter Hagedorn[b]

[a]*Department of Aerospace Engineering, Indian Institute of Technology Madras, Chennai 600036, India*
[b]*Department of Applied Mechanics, TU Darmstadt, Hochschulstrasse 1, 64289 Darmstadt, Germany*

Received 7 July 2006; received in revised form 11 September 2006; accepted 18 September 2006
Available online 9 November 2006

Abstract

Aeolian vibrations in the frequency range of 10–50 Hz are ubiquitous in the conductors of transmission lines. They are usually not perceptible to the casual observers due to their small amplitudes, nevertheless, they are important as they may lead to failure of the lines through material fatigue. These problems become more severe for long-span lines. Since the conductors are fabricated in finite lengths, every once in a while two conductors have to be connected in the field, using appropriate fittings. A particular case of fitting, considered in this paper, is the compression splice bushing (CSB), which is sometimes used in long spans to join the ends of two conductors. It is desired to estimate the values of the maximum bending stress developed in the conductors and in related fittings due to aeolian vibrations. An obvious approach would be to solve the boundary value problem for the conductors with the CSB; here a model is presented that avoids the solutions of the complete boundary value problem and results in solving a set of linear algebraic equations.

1. Introduction

Aeolian vibrations of the conductors of long span transmission lines have received much attention in Refs. [1–5]. The amplitudes of these vibrations are usually small as compared to the conductor diameters; nevertheless they are of major concern to the manufacturers of the transmission line conductors because they may lead to structural failure through material fatigue. It is important therefore to estimate the values of stresses occurring in the conductor and in related fittings due to aeolian vibrations so that adequate countermeasures can be taken as needed. This problem is particularly severe for long-span lines. In exceptional cases, e.g. due to topographic conditions, the span lengths may be as large as 3 km and above. Since the conductors are fabricated in finite lengths, every once in a while conductors' ends have to be connected in the field, using appropriate fittings (an alternative would be to make the connections at the ends only, i.e. at the tension towers). One of the several means of joining conductors' ends in the field is by means of compression splice bushing (CSB). During aeolian vibrations, bending stresses appear in the immediate neighborhood of the CSB, as at any fitting attached to the conductor. Also, the CSB itself is subjected to bending stresses, which may be critical for the reason that large deformations of the CSB and in the neighborhood

*Corresponding author. Tel.: +91 44 22574021; fax: +91 44 22574002.
E-mail address: nandan@ae.iitm.ac.in (N.K. Sinha).

0022-460X/$ - see front matter © 2006 Elsevier Ltd. All rights reserved.
doi:10.1016/j.jsv.2006.09.020

of the CSB may result in dislocation at the joints. In a long-span line the exact locations of the in-span fittings, in particular of the CSBs, are not accurately known, due to the relatively high tolerances; other non-constant parameters are, for example, the tension in the conductor, which depends on the temperature as well as on the mass per unit length which varies with a possible ice deposit in winter. These uncertainties in the physical model often result in questioning the viability of the mathematical models developed for computing parameters of such systems; the other problem being the amount of computational effort required.

The vibration amplitudes in the aeolian vibrations of a conductor are usually computed using the *energy balance principle* [6,7]. The bending stresses in the conductor far away from the ends (i.e. 'in the field') are a simple function of these amplitudes. The same applies for the (nominal) bending stresses in the conductors at the end (i.e. at the *suspension clamps*) and at all other points of the conductor, e.g. at the points of attachment of fittings (aircraft warning sphere, etc.). It is at the ends and at the in-span fittings that the highest bending stresses occur. In this paper, we compute the maximum possible bending stresses occurring in a CSB and in the neighborhood of the CSB as a function of the frequency and the phase angle, and compare them to the nominal bending stresses at the suspension clamps. Further, sensitivity analysis of the mathematical model with respect to change in mass density and tension in the conductors is done and maximum stress distribution along the span in the neighborhood of the CSB computed. The CSB in the present model is modeled as a short beam under large axial load, its bending stiffness is larger than that of the conductor, and the conductor is modeled as a taut string with bending stiffness. In order to compute bending stresses/strains in the CSB or in the conductor, the obvious approach would be to solve the boundary value problem for the conductor with the CSB followed by use of the *energy balance principle*. Here, a model is used which avoids the solutions of the complete boundary value problem [8] but considers only the CSB in an infinite span with a standing wave in the conductors far from the CSB. This is a realistic assumption since the tolerance in the placement of the CSB is normally high, so that its exact location in the field is not well known. The new approach results in a set of linear algebraic equations which can be solved easily.

2. Model description and solution approach

The schematic diagram in Fig. 1 represents two long-span conductors joined together by a CSB. The bushing is assumed to be tightly fitted to the conductors so that no slipping motion occurs, i.e. the friction force between the bushing and the conductor is greater than the normal forces developed at the interface due to bending of the conductor. As a first approximation here the conductor is assumed to be a solid of circular cross-section, and the bushing is a cylindrical tube of length $b(\ll L)$ (length of the conductor) with inner and outer radii R and R_B, respectively. R is also the radius of the conductor. For the purpose of calculation of stresses due to bending in the middle of the bushing, the three segments of the transmission line are marked 1, 2, 3 as shown in Fig. 1. Segments 1 and 3 are formed by the conductors only; 2 consists of the conductor with the bushing. Coordinates are as shown in Fig. 1. Material of the bushing is steel and that of the conductor is aluminum. Numerical data used in the computations are provided in Appendix. In the alternate solution approach, conductors with the CSB is modeled as an infinitely long string/beam as shown in Fig. 2 with standing sinusoidal waves at infinity ends.

2.1. Equation of motion and boundary conditions

For high-voltage overhead lines the conductors today typically consist of stranded metallic wires. The core normally is formed by steel wires (for structural reasons), while the outer layers are typically made of

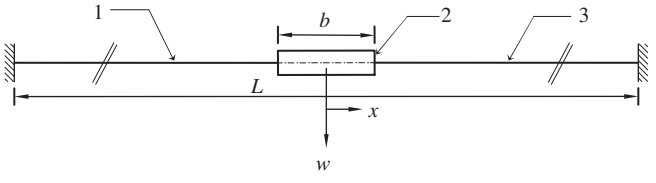

Fig. 1. A schematic of two conductors clamped at one ends and joined together at the other ends by a compression splice bushing.

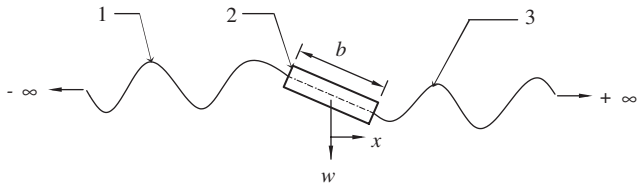

Fig. 2. A schematic of the two long conductors joined together by a compression splice bushing.

aluminum alloys (good conductivity!). This complex structure is however normally modeled as a taut string with mass per unit length $\mu = \rho A$, tensile force T and a (small) bending stiffness EI. ρ is the average density of the conductor material and A is the area of the cross-section. The conductor diameters d typically are of the order of a few centimeters and the wave lengths of the aeolian vibrations of a few meters. The maximum displacement amplitudes of the aeolian vibrations are normally well below one conductor diameter. These data justify modeling the conductor vibrations by means of the partial differential equation [9]:

$$\mathrm{EI}\, w_{xxxx}(x,t) + \mu w_{tt}(x,t) - T w_{xx}(x,t) = q(x,t,w,w_t) \tag{1}$$

corresponding to a taut string with bending stiffness, where $w(x, t)$ is the transverse deflection of the conductor at location x and at time t, and $q(x, t, w, w_t)$ represents external load as well as damping due to the hysteresis in the conductor and also due to the damping devices, if present. Variables with subscripts x and t indicate derivatives with respect to space and time, respectively.

A solution of the partial differential Eq. (1) for the free vibration of the conductor ($q(x, t, w, w_t) = 0$) can be obtained by using the method of separation of variables ($w(x, t) = W(x)\sin \omega t$) which results in the equation in space domain as

$$\mathrm{EI}\, W_{xxxx}(x) - T W_{xx}(x) - \rho A \omega^2 W(x) = 0, \tag{2}$$

where ω is the circular eigenfrequency of the conductor vibration.

Solution of Eq. (2), the transverse deflection $W(x)$ is

$$W(x) = A\mathrm{e}^{\alpha x} + B\mathrm{e}^{-\alpha x} + C \sin \beta x + D \cos \beta x \tag{3}$$

or

$$W(x) = A\mathrm{e}^{\alpha x} + B\mathrm{e}^{-\alpha x} + E \sin(\beta x + \phi), \tag{4}$$

where α and β are given by

$$\alpha = \sqrt{\frac{T + \sqrt{T^2 + 4\,\mathrm{EI}\,\rho A \omega^2}}{2\,\mathrm{EI}}}, \quad \beta = \sqrt{\frac{-T + \sqrt{T^2 + 4\,\mathrm{EI}\,\rho A \omega^2}}{2\,\mathrm{EI}}}. \tag{5}$$

Constants in Eq. (4) are to be determined from the physical boundary conditions. In the alternate solution approach, as explained earlier, two long conductors joined together by a CSB (Fig. 1) are considered to be equivalent to two infinitely long conductors connected by a CSB at one ends as shown in Fig. 2. Standing sinusoidal waves are assumed to be present far away from the CSB. This translates into the boundary conditions:

$$W(x) = S \sin\left(\frac{\pi x}{\lambda} - \phi\right) + \hat{w}(x); \;\; \lim_{x \to \pm\infty} \hat{w}(x) = 0, \tag{6}$$

where S is the amplitude of the standing harmonic wave, λ the wavelength, ϕ the phase angle, and $\hat{w}(x)$ consists of exponential terms in Eq. (4). In the problem to be solved here, we assume that bending stiffness of the conductor is not small but comparable to that of the bushing, so that, Eq. (1) holds true for all the three segments of the transmission line shown in Fig. 1. Tension is assumed to be constant throughout. The bending stiffness of the segment 2 is simple sum of the corresponding stiffnesses of the conductor and the bushing ($(\mathrm{EI})_2 = (\mathrm{EI})_1 + (\mathrm{EI})_{\mathrm{BUSHING}}$). The other boundary conditions are compatibility conditions, satisfying

continuity of displacement, slope, bending moment, and shear force at the bushing ends as follows:

$$\begin{aligned}
&w\left(\left(-\frac{b}{2}\right)^{-},t\right)=w\left(\left(-\frac{b}{2}\right)^{+},t\right), && w\left(\left(\frac{b}{2}\right)^{-},t\right)=w\left(\left(\frac{b}{2}\right)^{+},t\right),\\
&w_x\left(\left(-\frac{b}{2}\right)^{-},t\right)=w_x\left(\left(-\frac{b}{2}\right)^{+},t\right), && w_x\left(\left(\frac{b}{2}\right)^{-},t\right)=w_x\left(\left(\frac{b}{2}\right)^{+},t\right),\\
&(\mathrm{EI})_1 w_{xx}\left(\left(-\frac{b}{2}\right)^{-},t\right)=(\mathrm{EI})_2 w_{xx}\left(\left(-\frac{b}{2}\right)^{+},t\right), && (\mathrm{EI})_2 w_{xx}\left(\left(\frac{b}{2}\right)^{-},t\right)=(\mathrm{EI})_3 w_{xx}\left(\left(\frac{b}{2}\right)^{+},t\right),\\
&(\mathrm{EI})_1 w_{xxx}\left(\left(-\frac{b}{2}\right)^{-},t\right)=(\mathrm{EI})_2 w_{xxx}\left(\left(-\frac{b}{2}\right)^{+},t\right), && (\mathrm{EI})_2 w_{xxx}\left(\left(\frac{b}{2}\right)^{-},t\right)=(\mathrm{EI})_3 w_{xxx}\left(\left(\frac{b}{2}\right)^{+},t\right).
\end{aligned} \tag{7}$$

2.2. Stress computation

Using separation of variables, the boundary conditions (Eq. (7)) can be written as functions of the space variable x. From Eq. (5), it can be seen that α and β depend upon the local system parameters; hence, they are different for different sections of the conductor line in Fig. 1. Therefore, for the three segments of the conductor line depicted in Fig. 2, the transverse deflections are given by

$$\begin{aligned}
W_1(x) &= A_1 e^{\alpha_1 x} + B_1 e^{-\alpha_1 x} + E_1 \sin(\beta_1 x + \phi_1) \quad \text{for} \quad -\infty < x \leqslant -\frac{b}{2},\\
W_2(x) &= A_2 e^{\alpha_2 x} + B_2 e^{-\alpha_2 x} + E_2 \sin(\beta_2 x + \phi_2) \quad \text{for} \quad -\frac{b}{2} \leqslant x \leqslant +\frac{b}{2},\\
W_3(x) &= A_3 e^{\alpha_3 x} + B_3 e^{-\alpha_3 x} + E_3 \sin(\beta_3 x + \phi_3) \quad \text{for} \quad +\frac{b}{2} \leqslant x < +\infty,
\end{aligned} \tag{8}$$

where $\alpha_i = \sqrt{\left(T + \sqrt{T^2 + 4(\mathrm{EI})_i(\rho A)_i \omega^2}\right)/2(\mathrm{EI})_i}$ and $\beta_i = \sqrt{\left(-T + \sqrt{T^2 + 4(\mathrm{EI})_i(\rho A)_i \omega^2}\right)/2(\mathrm{EI})_i}$, $i = 1, 2, 3$. These deflections are required to satisfy the boundary conditions in Eqs. (6) and (7), which results in 8 linear non-homogeneous equations in 12 constants, A_i, B_i, E_i, ϕ_i ($i = 1, 2, 3$). B_1 and A_3 are zero due to the boundary conditions in Eq. (6). Among the remaining 10 constants, the amplitude E_1 (to be used as non-dimensionalizing variable), the circular frequency ω and the phase angle ϕ_1 of the standing wave at $x \to -\infty$ are arbitrarily chosen. The other 8 constants can be now determined uniquely from the 8 non-homogeneous linear algebraic equations as a function of the frequency ω and of E_1 and ϕ_1. This amounts to solving a matrix inversion problem

$$[\mathbf{G}]\widetilde{\mathbf{A}} = \widetilde{\mathbf{B}}, \tag{9}$$

where $\widetilde{\mathbf{A}}$ is the vector of constants to be determined and the constant vector $\widetilde{\mathbf{B}}$ on the right-hand side results from the boundary conditions. $\mathbf{G}$, $\widetilde{\mathbf{A}}$, and $\widetilde{\mathbf{B}}$ are given in Appendix. With the known constants, the maximum bending stress $\sigma(0)$ at $x = 0$, i.e. in the middle of the bushing, can be calculated from the bending moment amplitude at this point, which is given by

$$M(0) = -(\mathrm{EI})_2 W_{2xx}(0). \tag{10}$$

The stress amplitude at $x = 0$ is

$$\sigma_B = \sigma(0) = \frac{M(0)}{I_{\mathrm{EQ}}} R_B, \tag{11}$$

where R_B is the outer radius of the bushing and I_{EQ} is the equivalent moment of inertia of the segment 2. I_{EQ} is given by [10]

$$I_{\mathrm{EQ}} = \frac{\pi a h^3}{4} + \frac{\pi\left(R_B^4 - R^4\right)}{4}, \tag{12}$$

where $a = (E_{\mathrm{BUSHING}}/E_{\mathrm{CONDUCTOR}})h$ and $h = R$. The stress amplitude $\sigma(0)$ is a function of the circular frequency ω and of the phase angle ϕ_1 and is also linear function of the amplitude of the standing wave E_1 at the left infinity end. The dependence on E_1 can however be eliminated by normalizing $\sigma(0)$ with a reference

stress, e.g. with the stress amplitude occurring at the rigid clamp end of a conductor oscillating in the form of a harmonic standing wave with amplitude E_1 far away from the suspension clamp, according to Fig. 3. The transverse deflection of the conductor is

$$W(x) = Ce^{\alpha x} + De^{-\alpha x} + E_1 \sin(\beta x + \phi). \tag{13}$$

where $C = 0$ due to the sinusoidal standing wave boundary condition at the right infinity end, and the boundary conditions at the clamped end, $W(0) = 0$ and $W_x(0) = 0$ result in

$$\tan \phi = -\frac{\beta(\omega)}{\alpha(\omega)}. \tag{14}$$

The maximum bending stress at the clamped end is therefore given by

$$\sigma_C = E_1 \beta \sqrt{\alpha^2 + \beta^2} (\mathrm{EI})_1 \frac{R}{I_1} \tag{15}$$

as a function of E_1 and ω. Here $(\mathrm{EI})_1$ is the bending stiffness of the conductor, and I_1 is its moment of inertia and R its radius.

Since both σ_B and σ_C depend linearly on E_1, the normalized stress at the CSB, namely σ_B/σ_C, no longer depends on E_1 but only on the phase angle ϕ_1 and the circular frequency $\omega = 2\pi f$. Fig. 4 shows σ_B/σ_C as a function of ϕ_1 (in the range $-\pi$ to π radians) and f (in the range 10–50 Hz). Non-dimesionalized stress plot indicates the relative magnitudes of the stresses occurring in the bushing as compared to that occurring at the clamped ends. In Fig. 5, the maximum values of σ_B/σ_C over the phase angle ϕ_1 is shown as a function of f, which suggests that maximum stress occurring in the bushing is approximately 25% of that occurring at the clamped ends. This maximization makes sense, because the phase angle ϕ_1 can in this simple model assume any value. The non-dimensional bending stresses in the bushing therefore represent the worst possible case of the stresses in the CSB (whose exact location in the conductors is not really known due to the existing tolerances). Fig. 6 plots the span wise distribution of the maximum bending stresses on and in the neighborhood of the CSB. It can be seen from Fig. 6 that maximum bending stress occurs in the neighborhood of the CSB at a distance of the CSB length ($x = -b$), while in the CSB itself maximum bending stress occurs at $x = 0$. The maximum bending stress occurring in the

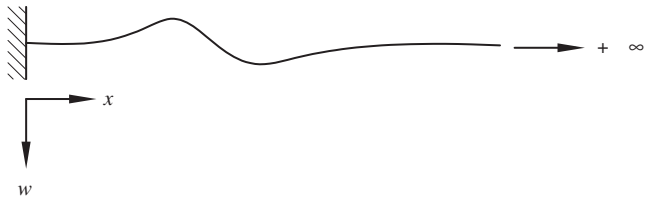

Fig. 3. A schematic of an infinitely long conductor clamped at one end.

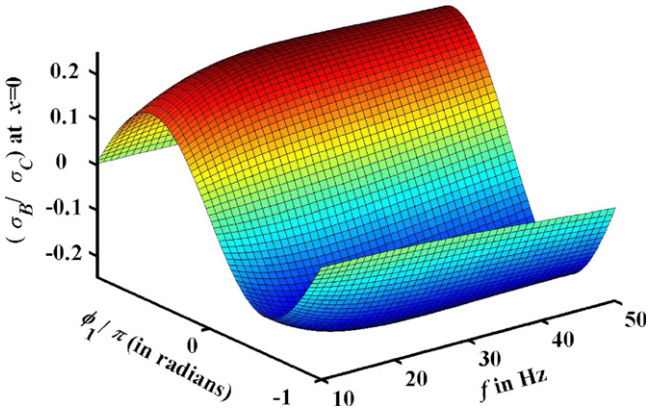

Fig. 4. Plot of maximum bending stress occurring in the CSB as a function of the frequency and the phase angle normalized with the maximum bending stress developed at the clamped end (for tension $T = \text{const.}$, mass density of the junction $\mu_2 = \text{const.}$).

conductor (at $x = -b$) is about 60% of that occurring at the clamp ends; this suggests that maximum likelihood of failure of the conductor is at the clamp ends. However, due to large deformation in the neighborhood of the CSB, the joint with CSB may itself undergo unwanted deformations.

Furthermore, a sensitivity analysis of the proposed model is done with respect to the uncertainties present in the physical system, for example, the tension in the conductor, and the change in the mass of the junction due to possible deposition of ice in winter. Results have been produced for $\pm 10\%$ variations in the tension and up to 15% change in the mass density $\mu_2 = (\rho A)_2$ of the junction. Results plotted in Figs. 7 and 8 clearly suggest that there is no significant variation in the non-dimensional values of the maximum stress in the frequency range 10–50 Hz over the phase angle $-\pi$ to π radians with the uncertainties due to variations in tension in the CSB and the mass of the junction. Variation in maximum bending stress occurring in the center of the CSB with respect to change in length of the CSB (considered here as uncertainties in the model) is shown in Fig. 9 as function of frequency. The change is again not large here, though, for larger lengths of the CSB appreciable variations in the maximum bending stress have been noticed.

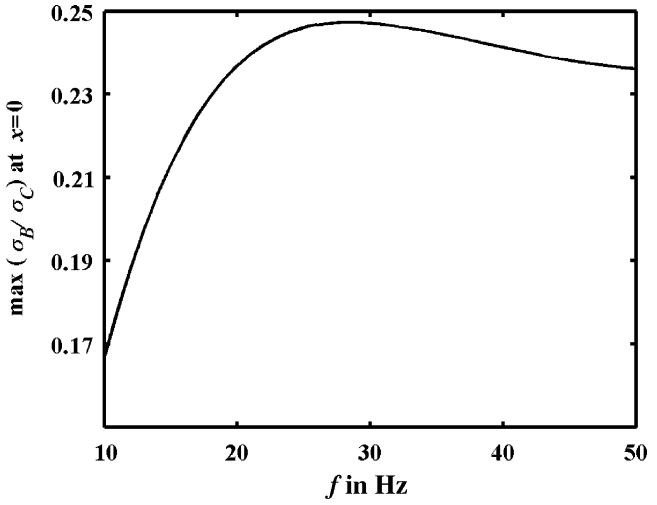

Fig. 5. Plot of maximum bending stress occurring in the CSB as a function of frequency normalized with the maximum bending stress developed at the clamped end (for tension $T = \text{const.}$, mass density of the junction $\mu_2 = \text{const.}$).

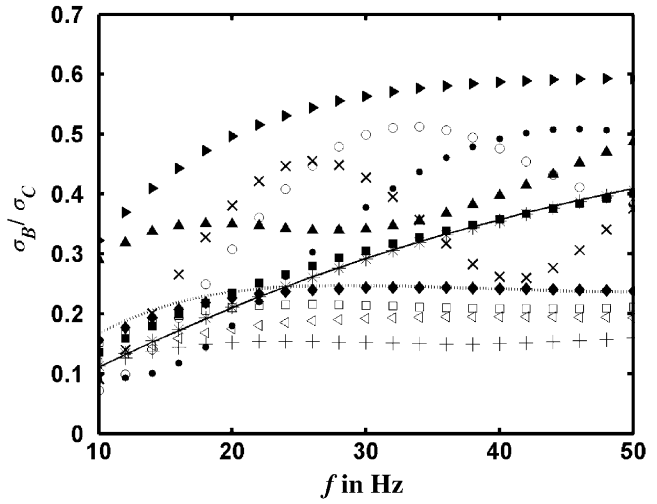

Fig. 6. Plot of maximum bending stress occurring in the line at different locations from the center of the bushing as a function of frequency normalized with the maximum bending stress developed at the clamped end (for tension $T = \text{const.}$, mass density of the junction $\mu_2 = \text{const.}$) (- - -: $x = 0$, ♦: $x = -b/4$, ◁: $x = -b/2$, ▶: $x = -b$, ■: $x = -2b$, ∗: $x = -3b$, : $x = -4b$, □: $x = b/4$, +: $x = b/2$, ▲: $x = b$, ●: $x = 2b$, $x = 3b$, ×: $x = 4b$).

3. Concluding remarks

Stresses and strains occurring in vortex excited oscillations of the conductors of long span overhead transmission lines with in-span fittings can be estimated using the energy balance principle in its modified form as described in Ref. [9]. In this approach, first the eigenvalue problem for the system is solved. The spectrum being very dense, it is then assumed that the forced vibrations always occur in resonance and that the vibration shape is one of the corresponding eigenmodes. Only a scaling of the amplitude is therefore necessary to determine the vibration amplitudes for any given (eigen) frequency and this is done using the *energy balance principle*, where the average wind-power input is set equal to the power dissipated due to damping in the conductor itself and also in the damping devices, if present. With these known vibration amplitudes, the bending strains and stresses, both in the conductor and also in the fittings themselves can be computed. In particular, the stresses in a CSB could be calculated in this manner.

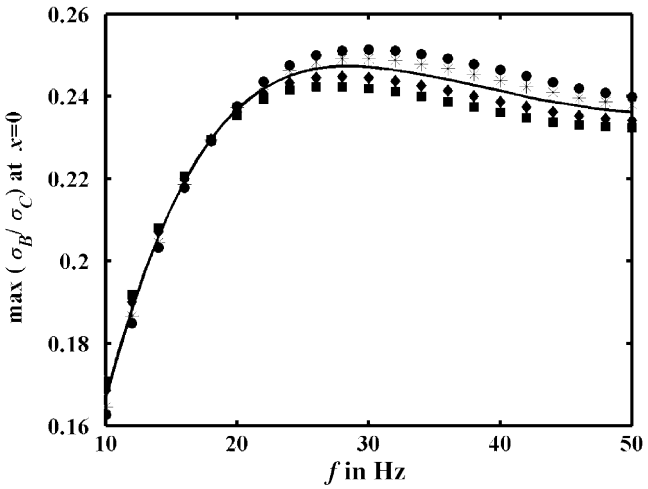

Fig. 7. Plot of maximum bending stress occurring in the CSB as a function of frequency normalized with the maximum bending stress developed at the clamped end (for varying tension T, mass density of the junction $\mu_2 = \text{const.}$) (—: T, ■: 0.9 T, ◆: 0.95 T, ∗: 1.05 T, ●: 1.1 T).

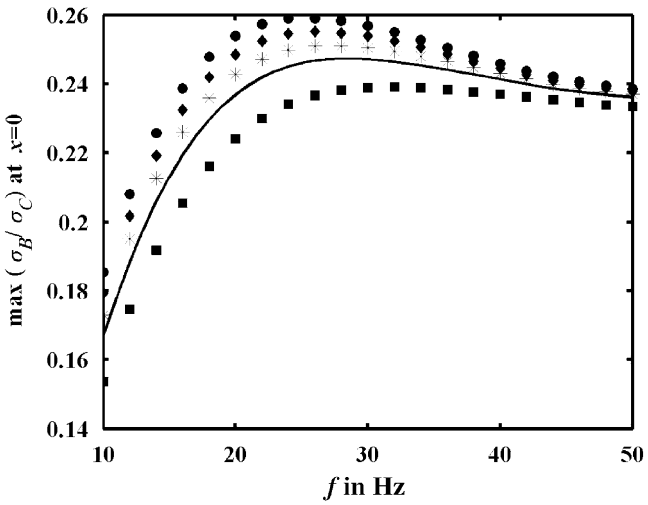

Fig. 8. Plot of maximum bending stress occurring in the CSB as a function of frequency normalized with the maximum bending stress developed at the clamped end (for tension $T = \text{const.}$, mass density of the junction μ_2 varying) (—: μ_2, ■: $0.9\mu_2$, ∗: $1.05\mu_2$, ◆: $1.1\mu_2$, ●: $1.15\mu_2$).

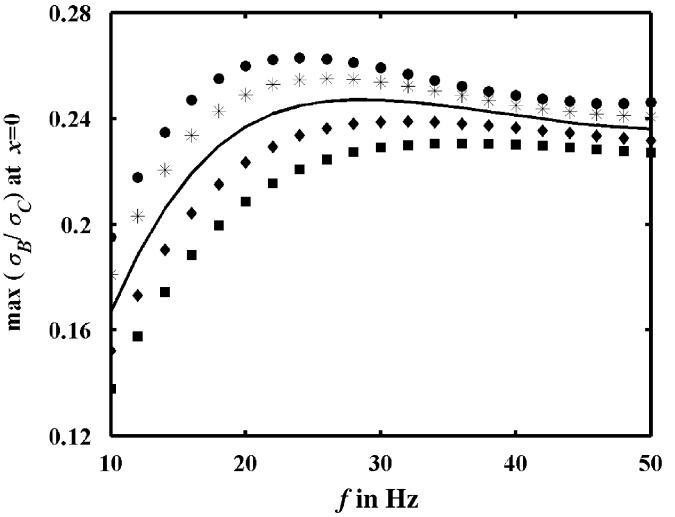

Fig. 9. Plot of maximum bending stress occurring in the CSB as a function of frequency normalized with the maximum bending stress developed at the clamped end (for tension $T = \text{const.}$, mass density of the junction $\mu_2 = \text{const.}$) (for varying CSB length, ■: $b = 0.36\,\text{m}$, ◆: $b = 0.4\,\text{m}$, —: $b = 0.44\,\text{m}$, ∗: $b = 0.48\,\text{m}$, ●: $b = 0.52\,\text{m}$).

The eigenvalues are however quite sensitive to the parameters of the system such as the tension in the conductor which is a function of the temperature, the location of the CSB in the conductor which is only specified within a relatively large tolerance, etc. In the alternative approach presented in this paper, the solution of the eigenvalue problem is avoided and for a long conductor the maximum possible bending stress is estimated by considering standing waves of a given amplitude and an arbitrary phase with respect to the spatial variable. The bending stress in the compression bushing for each vibration amplitude is maximized with respect to the phase and is normalized with respect to the bending stress in the conductor at the clamp end. Since both bending stresses are linear in the amplitude, the stress in the bushing normalized in this manner no longer depends on the amplitude. On the other hand, permissible values for the nominal bending stresses in the conductor at the ends in very long conductors are routinely estimated via energy balance. They are also measured in the field indirectly by obtaining the 'bending amplitude' via 'vibration recorder' [2]. A similar procedure can be used to estimate the relative values of the bending stresses at other fittings in long span conductors.

Appendix

Conductor data:

$E_{\text{CONDUCTOR}}$ (aluminum) $= 70 \times 10^9\,\text{N m}^{-2}$,
$(\text{EI})_1 = (\text{EI})_3 = 584.3\,\text{N m}^2$,
$\text{T} = 12630\,\text{N}$,
$\rho_{\text{Al}} = 70 \times 10^9\,\text{kg m}^{-3}$,
$R = 0.0102\,\text{m}$.

Bushing data:

E_{BUSHING} (steel) $= 200 \times 10^9\,\text{N m}^{-2}$,
$(\text{EI})_2 = 1.22 \times 10^4\,\text{N m}^2$,
$T = 12630\,\text{N}$,
$\rho_{\text{steel}} = 7860\,\text{kg m}^{-3}$,
$R_{\text{OUT}} = R_{\text{B}} = 0.0173\,\text{m}$,
$R_{\text{IN}} = R = 0.0102\,\text{m}$,
$b = 0.44\,\text{m}$.

The vectors $\widetilde{\mathbf{A}}$, and $\widetilde{\mathbf{B}}$ and the matrix $\mathbf{G}$ in Eq. (9) are

$$\widetilde{\mathbf{A}} = \left[A_1, A_2, B_2, E_2 \cos\,\phi_2, E_2 \sin\,\phi_2, B_3, E_3 \cos\,\phi_3, E_3 \sin\,\phi_3\right]' \tag{16}$$

$$\widetilde{\mathbf{B}} = \left[-E_1\,\sin\left(-\frac{\beta_1 b}{2}+\phi_1\right),\ 0,\ -E_1\beta_1\,\cos\left(-\frac{\beta_1 b}{2}+\phi_1\right),\ 0,\ (\mathrm{EI})_1\beta_1^2 E_1\,\sin\left(-\frac{\beta_1 b}{2}+\phi_1\right),\ 0,\ (\mathrm{EI})_1\beta_1^3 E_1\,\cos\left(-\frac{\beta_1 b}{2}+\phi_1\right), 0\right]' \tag{17}$$

$$G = \begin{bmatrix}
e^{-\frac{\alpha_1 b}{2}} & -e^{-\frac{\alpha_2 b}{2}} & -e^{\frac{\alpha_2 b}{2}} & -\sin\left(-\frac{\beta_2 b}{2}\right) & -\cos\left(-\frac{\beta_2 b}{2}\right) & 0 & 0 & 0 \\
0 & e^{\frac{\alpha_2 b}{2}} & e^{-\frac{\alpha_2 b}{2}} & \sin\left(\frac{\beta_2 b}{2}\right) & \cos\left(\frac{\beta_2 b}{2}\right) & -e^{-\frac{\alpha_3 b}{2}} & -\sin\left(\frac{\beta_3 b}{2}\right) & -\cos\left(\frac{\beta_3 b}{2}\right) \\
\alpha_1 e^{-\frac{\alpha_1 b}{2}} & -\alpha_2 e^{-\frac{\alpha_2 b}{2}} & \alpha_2 e^{\frac{\alpha_2 b}{2}} & -\beta_2\,\cos\left(-\frac{\beta_2 b}{2}\right) & \beta_2\,\sin\left(-\frac{\beta_2 b}{2}\right) & 0 & 0 & 0 \\
0 & \alpha_2 e^{\frac{\alpha_2 b}{2}} & -\alpha_2 e^{-\frac{\alpha_2 b}{2}} & \beta_2\,\cos\left(\frac{\beta_2 b}{2}\right) & -\beta_2\,\sin\left(\frac{\beta_2 b}{2}\right) & \alpha_3 e^{-\frac{\alpha_3 b}{2}} & -\beta_3\,\cos\left(\frac{\beta_3 b}{2}\right) & \beta_3\,\sin\left(\frac{\beta_3 b}{2}\right) \\
(\mathrm{EI})_1\alpha_1^2 e^{-\frac{\alpha_1 b}{2}} & -(\mathrm{EI})_2\alpha_2^2 e^{-\frac{\alpha_2 b}{2}} & -(\mathrm{EI})_2\alpha_2^2 e^{\frac{\alpha_2 b}{2}} & (\mathrm{EI})_2\beta_2^2\,\sin\left(-\frac{\beta_2 b}{2}\right) & (\mathrm{EI})_2\beta_2^2\,\cos\left(-\frac{\beta_2 b}{2}\right) & 0 & 0 & 0 \\
0 & (\mathrm{EI})_2\alpha_2^2 e^{\frac{\alpha_2 b}{2}} & (\mathrm{EI})_2\alpha_2^2 e^{-\frac{\alpha_2 b}{2}} & -(\mathrm{EI})_2\beta_2^2\,\sin\left(\frac{\beta_2 b}{2}\right) & -(\mathrm{EI})_2\beta_2^2\,\cos\left(\frac{\beta_2 b}{2}\right) & -(\mathrm{EI})_3\alpha_3^2 e^{-\frac{\alpha_3 b}{2}} & (\mathrm{EI})_3\beta_3^2\,\sin\left(\frac{\beta_3 b}{2}\right) & (\mathrm{EI})_3\beta_3^2\,\cos\left(\frac{\beta_3 b}{2}\right) \\
(\mathrm{EI})_1\alpha_1^3 e^{-\frac{\alpha_1 b}{2}} & -(\mathrm{EI})_2\alpha_2^3 e^{-\frac{\alpha_2 b}{2}} & (\mathrm{EI})_2\alpha_2^3 e^{\frac{\alpha_2 b}{2}} & (\mathrm{EI})_2\beta_2^3\,\cos\left(-\frac{\beta_2 b}{2}\right) & -(\mathrm{EI})_2\beta_2^3\,\sin\left(-\frac{\beta_2 b}{2}\right) & 0 & 0 & 0 \\
0 & (\mathrm{EI})_2\alpha_2^3 e^{\frac{\alpha_2 b}{2}} & -(\mathrm{EI})_2\alpha_2^3 e^{-\frac{\alpha_2 b}{2}} & -(\mathrm{EI})_2\beta_2^3\,\cos\left(\frac{\beta_2 b}{2}\right) & (\mathrm{EI})_2\beta_2^3\,\sin\left(\frac{\beta_2 b}{2}\right) & -(\mathrm{EI})_3\alpha_3^3 e^{-\frac{\alpha_3 b}{2}} & (\mathrm{EI})_3\beta_3^3\,\cos\left(\frac{\beta_3 b}{2}\right) & -(\mathrm{EI})_3\beta_3^3\,\sin\left(\frac{\beta_3 b}{2}\right)
\end{bmatrix} \tag{18}$$

References

[1] R. Claren, G. Diana, Mathematical analysis of transmission line vibration, *IEEE Transactions on Power Apparatus and Systems* 88 (1969) 1741–1771.
[2] EPRI, *Transmission Line Reference Book, Wind Induced Conductor Motion*, Electrical Power Research Institute, Palo Alto, CA, 1979.
[3] M.S. Dhotarad, N. Ganesan, B.V.A. Rao, Transmission line vibration, *Journal of Sound and Vibration* 60 (1978) 217–327.
[4] P. Hagedorn, On the computation of damped wind excited vibrations of overhead transmission lines, *Journal of Sound and Vibration* 83 (2) (1982) 253–271.
[5] J.G. Allnut, M.D. Rowbottom, Damping of aeolian vibration on overhead lines by vibration dampers, *Proceedings of the Institute of Electrical and Electronic Engineers* 121 (1974) 1175–1178.
[6] K.V. Singh, Y.M. Ram, Transcendental eigenvalue problem and its applications, *AIAA Journal* 40 (2002) 1402–1407.
[7] M. Ervik, Estimating aeolian vibration level based on energy balance principle, *CIGRE SC-22, WG* (1975).
[8] E. Bahtovska, The energy balance for damped wind-excited vibrations, *Facta Universitatis* 1 (7) (2000) 769–773.
[9] H. Verma, P. Hagedorn, Wind induced vibrations of long electrical overhead transmission line spans: a modified approach, *Wind and Structures* 8 (2) (2005) 89–106.
[10] E.P. Popov, *Introduction to Mechanics of Solids*, Prentice-Hall Inc., Englewood Cliffs, NJ, 1968.